NANO LETTERS

2003
Vol. 3, No. 8
1155−1161

Ultrathin, Protective Coatings of Poly(*o*-phenylenediamine) as Electrochemical Proton Gates: Making Mesoporous MnO_2 Nanoarchitectures Stable in Acid Electrolytes

Jeffrey W. Long,* Christopher P. Rhodes, Amanda L. Young, and Debra R. Rolison*

Naval Research Laboratory, Surface Chemistry Branch, Code 6170, 4555 Overlook Avenue, SW, Washington, D.C. 20375-5320

Received May 30, 2003

ABSTRACT

We have created hybrid organic–inorganic nanoarchitectures by electrodepositing ultrathin (<10-nm-thick) polymer coatings onto nanostructured MnO_2 birnessite-type electrodes with surface areas in excess of 200 $m^2\ g^{-1}$. By choosing a self-limited growth process, based on the electropolymerization of *o*-phenylenediamine, the resulting polymer conformally coats the oxide nanoscale network without disrupting the continuous mesoporosity of the initial MnO_2 nanoarchitecture. These polymer coatings serve as pinhole-free physical barriers to external, acidic electrolyte, specifically, H_2O and hydrated protons, and protect the underlying MnO_2 nanoarchitecture from dissolution. The underlying metal oxide remains electrochemically addressable via an electrochemical proton-gating mechanism in which charge-compensating unsolvated protons are transported through the polymer coating. The 3D-templated electrochemical fabrication of polymer at an electrified metal oxide nanoarchitecture provides a new model for the development of electrochemical capacitors based on hybrid configurations using low-cost metal oxides such as MnO_2.

Introduction. We have previously demonstrated the importance of interconnected porosity—"nothingness"[1]—in nanoarchitectures designed for rate-critical measurements and applications, including sensing[2] and the electrocatalyzed oxidation of fuel.[3] High-quality "nothing" is also critical when the application requires chemical modification of the interior of the nanoarchitecture. Control of the fabrication process is often facilitated in aerogel (and related ambigel) nanoarchitectures because these sol−gel-derived, ultraporous materials, which combine bicontinuous networks of nanoscale solid domains and aperiodic mesoporosity,[4,5] permit facile mass transport of reactants (molecules, ions, and nanoscopic objects such as colloids) and byproducts throughout the architecture. Postsynthetic modification of aerogels can range from etching away anisotropically aligned magnetic particles (to create anisotropically aligned macropores)[6] to laying down a 4-nm-wide conformal electron path within silica aerogels[7] to grafting hydrophobic functionalities onto titania aerogels.[8]

When charge insertion into the solid state controls the rate-critical application, as in batteries, electrochromics, and electrochemical capacitors, expressing electrically conductive transition-metal oxides as nanoarchitectures enhances electrochemical performance.[5] These nanoarchitectural oxides are ideal electrode structures that massively amplify the electrode/electrolyte interface such that their extensive free volume of interconnected porosity facilitates the transport of charge-compensating cations to the high-surface-area electrified oxide. The nanoscale dimensions of the oxide domains also minimize the distances over which insertion cations diffuse via slow solid-state mechanisms. This combination of properties allows these oxide nanoarchitectures to achieve high electrode charge−discharge rates while also retaining high energy density, thus exhibiting the best individual characteristics of both capacitors and batteries.

Manganese oxide aerogels and ambigels exhibit substantial improvements as nonaqueous[9−11] and aqueous[12] cation-insertion materials, but the instability of MnO_2 in acidic electrolytes limits its application in electrochemical capacitors. Previous studies with hydrous RuO_2 (with specific capacitances as high as 720 $F\ g^{-1}$ [13]) have demonstrated that

* Corresponding authors. E-mail: jwlong@ccs.nrl.navy.mil; rolison@nrl.navy.mil.

10.1021/nl0343598 CCC: $25.00
Published on Web 07/12/2003

the maximum specific capacitance is achieved in acidic electrolytes, where high concentrations of highly mobile protons are available to the oxide electrode.[14,15] Manganese oxide undergoes a reductive-dissolution process when exposed to even mildly acidic electrolytes, yielding water-soluble Mn(II) species.[16−18] The use of MnO_2 has been limited, therefore, to near-neutral- and basic-pH aqueous electrolytes where the specific capacitance is diminished by the presence of less-desirable insertion cations such as Li^+ and K^+, which compete with H^+ for association at the MnO_2 electrode.

We now report a strategy to stabilize MnO_2 nanoarchitectures in aqueous acid by electrodepositing protective polymer coatings in which growth occurs only at the nanostructured electrified surface. We adapt previously reported methods for the oxidative electropolymerization of *o*-phenylenediamine (OPD)[19−21] as a means to apply ultrathin, conformal poly(*o*-phenylenediamine) (PPD) coatings onto nanostructured MnO_2 ambigel electrodes with surface areas in excess of 200 $m^2\ g^{-1}$.[22] These hybrid organic−inorganic nanoarchitectures are stable in aqueous acid electrolytes, even upon electrochemical cycling.

Background. Electrochemical capacitors are a general class of energy-storage materials that bridge the performance gap between the high energy density of batteries and the high power density derived from dielectric capacitors.[23,24] At present, high-performance electrochemical capacitors (also denoted as ultracapacitors) are based on nanoscale forms of mixed ion−electron conducting disordered, hydrous metal oxides, such as hydrous ruthenium oxide ($H_xRu^{III}_xRu^{IV}_{1-x}O_2$ or $RuO_2{\cdot}xH_2O$), that store charge via a cation−electron insertion mechanism (eq 1).

$$H_xRu^{III}_xRu^{IV}_{1-x}O_2 + ye^- + yH^+ \rightleftharpoons H_{x+y}Ru^{III}_{x+y}Ru^{IV}_{1-x-y}O_2 \quad (1)$$

The high cost of ruthenium, a platinum-group metal, limits its utilization. Manganese oxides, which have been extensively investigated as ion-insertion cathode materials for energy storage, ranging from alkaline Zn/MnO_2 cells[25] to lithium ion batteries,[26] are being explored as an economical and environmentally benign alternative to RuO_2. Specific capacitance values as high as 700 F g^{-1} are reported,[27] although more practical electrode constructions yield only 200 F g^{-1}.[12,28,29]

Electropolymerized films on electrodes have been extensively studied as passivating coatings, especially for corrosion protection.[30] The structure and properties of one such polymer, poly(*o*-phenylenediamine (PPD), depend strongly on the pH of the aqueous electrolyte used to oxidize the OPD monomer.[31] Poly(*o*-phenylenediamine) synthesized from strongly acidic solutions exhibits a phenazine-like structure (Scheme 1)[32] and can be grown to >1-μm-thick films with moderate conductivity (10^{-4}−10^{-2} S cm^{-1}).[32,33] In contrast, when PPD is electrodeposited from aqueous electrolytes with pH > 1, insulating, ultrathin (typically <10-nm-thick) coatings are formed. Under these conditions, the structure

Scheme 1. Idealized Chemical Structures of Poly(*o*-phenylenediamine) in Its Fully Oxidized Form

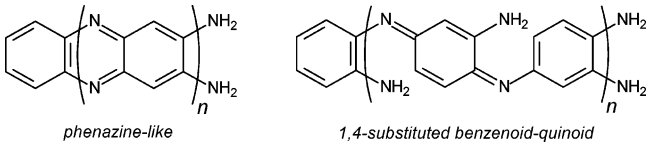

of the polymer backbone is disrupted by the presence of 1,4-substituted benzenoid−quinoid defects,[31] which likely diminish the electronic conductivity of the polymer. Although benzenoid−quinoid defects are present in all OPD-derived polymers, they become more prevalent as the pH of the initial monomer solution increases.[31] Electropolymerization of *o*-phenylenediamine has been used to passivate such semiconductor electrode structures as WO_3[34] and WSe_2,[21] although the stability of the coated semiconductors in acid electrolyte was not reported.

For potential use in ultracapacitors that are designed around hybrid polymer−metal oxide nanoarchitectures, the polymer coating must be uniformly distributed over the nanostructured oxide electrode without occluding or filling the mesoporous network. The pore volume of MnO_2 ambigels is centered in ∼25-nm pores with further distribution in the 10−80 nm range,[22] which is a size range that balances the facile diffusion of redox solutes and solvated ions with the exposure of solutes to the "walls" of the nanoarchitecture.

Electropolymerizing Self-Limited Films of Poly(*o*-phenylenediamine). Self-limited PPD films, electrodeposited from a pH 9 aqueous borate buffer at planar indium−tin oxide (ITO) electrodes, have a thickness of 7−9 nm, as directly measured using tapping-mode atomic force microscopy.[35] As expected, the insulating nature of the growing PPD polymer results in self-limiting film formation at this pH.[20] These values are also in agreement with previous estimates of film thickness on Pt by Losito et al., as determined by X-ray photoelectron spectroscopy.[31]

The electropolymerization of *o*-phenylenediamine at a nanostructured, ITO-supported MnO_2 ambigel electrode under voltammetric conditions is illustrated in Figure 1a. The oxidation of OPD monomer to the radical cation commences at ca. +0.25 V (vs Ag/AgCl), which initiates the formation of oligomers and polymers. On the second and third voltammetric sweeps, the oxidation current diminishes until by the fourth cycle no significant change in current is observed. As with planar electrodes, the electropolymerization of OPD at MnO_2 ambigel electrodes is a self-limiting process, where the MnO_2 electrode quickly passivates toward further oxidation of OPD monomers or oligomers. Potential-pulse deposition methods, which ensure a replenishing flux of monomers throughout the pore network during the "off" portion of the duty cycle, permit greater control of the electropolymerization than does voltammetry (Figure 1b). We achieve high-quality PPD coatings on the MnO_2 nanoarchitecture by pulsing between oxidizing (+1.0 V) and rest (0 V) potentials.

Native (uncoated) MnO_2 ambigel films exhibit a highly porous architecture, as seen by scanning electron microscopy

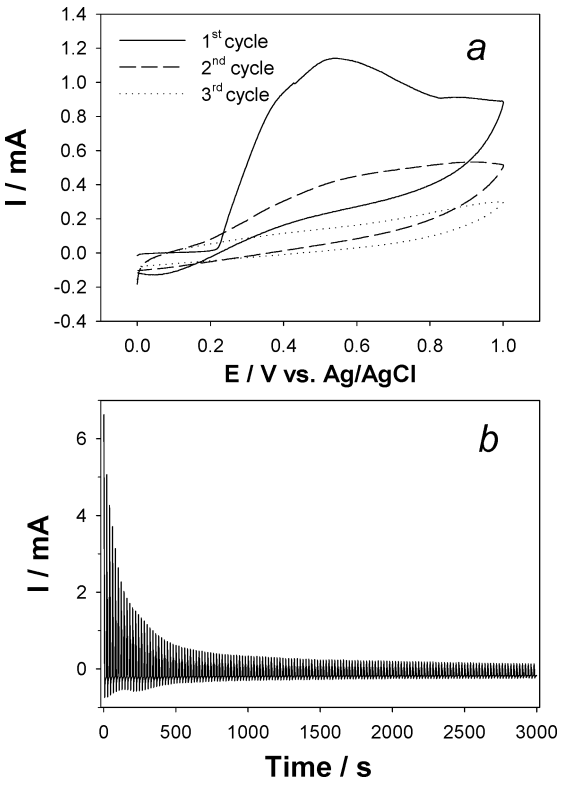

Figure 1. Electropolymerization of *o*-phenylenediamine at ITO-supported MnO_2 ambigel electrodes: (a) under voltammetric conditions with a scan rate of 10 mV s^{-1}; (b) under potential-pulse conditions with a 5-s oxidation pulse at +1.0 V followed by a 15-s rest pulse at 0 V, with a total of 200 pulse cycles. In both cases, the electrolyte contains 10 mM *o*-phenylenediamine, 0.2 M Na_2SO_4, and 50 mM borate buffer (pH 9.1), prepared in 18 MΩ cm water.

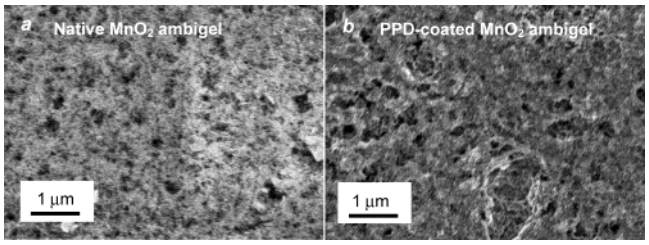

Figure 2. Scanning electron micrographs for a native MnO_2 ambigel film and a MnO_2 ambigel film onto which OPD has been electrochemically polymerized via a potential-pulse deposition.

(Figure 2a). The PPD-coated MnO_2 ambigel retains a significant degree of the initial porous structure of the uncoated oxide (Figure 2b). Although some of the fine structure is obscured in this micrograph, the loss of resolution may arise more from a decrease in conductivity at this surface due to the polymer coating and the lack of an overcoat of gold rather than from the polymer carpeting over nanoscale features. We observe similar morphological trends with atomic force microscopy imaging.[36]

Behavior of MnO_2 and PPD-MnO_2 Nanoarchitectures in Acid. Prior to evaluating polymer-coated MnO_2 nanoarchitectures in acidic electrolyte, we first consider the electrochemical behavior of native uncoated MnO_2 films. Reductive dissolution is initiated by reducing manganese (IV)

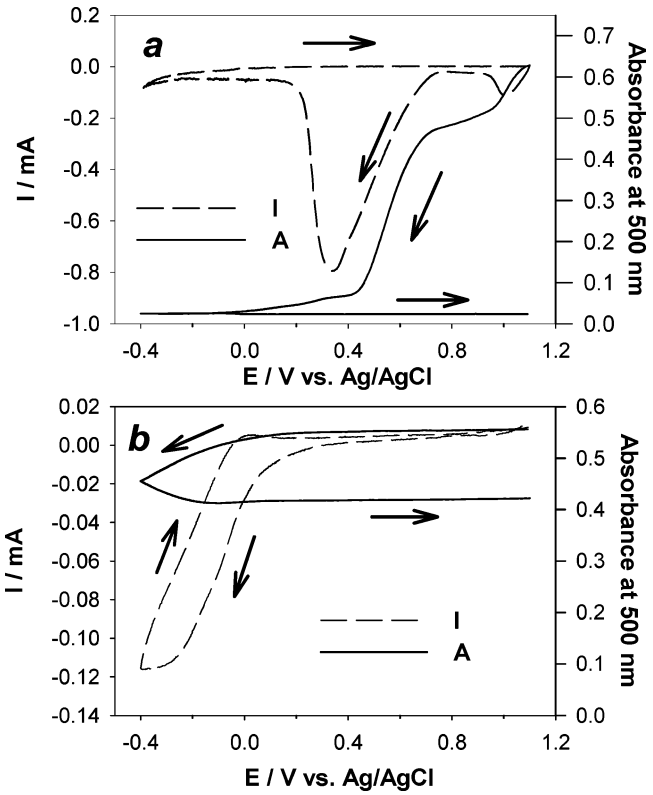

Figure 3. First-cycle voltammograms for ITO-supported ambigel films of (a) native MnO_2 and (b) PPD-coated MnO_2: (- - -) electrochemical current; (—) spectroscopic absorbance at 500 nm. Measurements are performed in 0.1 M H_2SO_4 at a scan rate of 4 mV s^{-1}. In the case of the PPD-coated MnO_2, the initial electropolymerization is performed by the potential-pulse method.

sites within the oxide to Mn(III) (with an accompanying insertion of protons from the acidic electrolyte).

$$Mn^{IV}O_2 + H^+ + e^- \rightleftharpoons Mn^{III}OOH \qquad (2)$$

Manganese(III) sites may be further reduced, as in eq 3, or undergo disproportionation, as in eq 4.

$$Mn^{III}OOH + 3H^+ + e^- \rightarrow Mn(II)(aq) + 2H_2O \qquad (3)$$

$$2Mn^{III}OOH + 2H^+ \rightarrow Mn^{IV}O_2 + Mn(II)(aq) + 2H_2O \qquad (4)$$

In either case, the overall reaction may written as

$$Mn^{IV}O_2 + 4H^+ + 2e^- \rightarrow Mn(II)(aq) + 2H_2O \qquad (5)$$

with the initial MnO_2 solid reduced to soluble Mn(II) species. Redeposition of MnO_2 via electro-oxidation of Mn(II) is inhibited in acid electrolytes, requiring high overpotentials and elevated temperatures to achieve significant deposition rates.[18]

Electrochemical dissolution in acid electrolytes is exacerbated at high-surface-area forms of MnO_2, as seen in the cyclic voltammogram in Figure 3a for an ITO-supported birnessite-MnO_2 ambigel film.[22] This measurement is per-

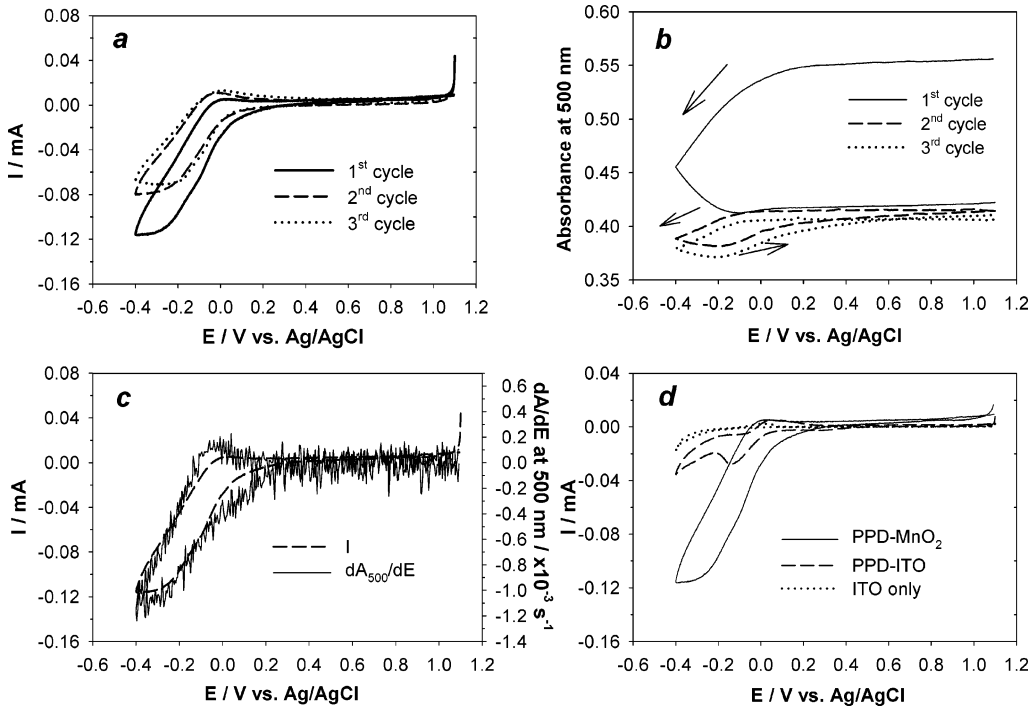

Figure 4. (a) Voltammograms for ITO-supported PPD-coated MnO_2 ambigel films for the first three cycles; (b) corresponding spectroscopic absorbance at a wavelength of 500 nm recorded simultaneously during the first three voltammetric cycles; (c) voltammogram and differential absorbance ($\partial A_{500}/\partial t$) at 500 nm for the first voltammetric cycle of PPD-coated MnO_2; (d) comparison of first-cycle voltammograms for PPD-coated MnO_2 (−), a PPD film on ITO (- - -), and a clean ITO slide (···). All measurements are performed in 0.1 M H_2SO_4 at a scan rate of 4 mV s^{-1}.

formed in a spectroelectrochemical cell so that the optical absorbance of the MnO_2 film can be monitored simultaneously during the voltammetric scan. Manganese oxide is an anodically coloring electrochromic oxide, where the optical absorbance is primarily assigned to the Mn(IV) oxidation state.[37,38] Thus, spectroelectrochemical measurements provide an in-situ, temporal measure of the electronic state of the MnO_2 film during electrochemical cycling. Reduction of the MnO_2 film proceeds in multiple steps with peaks at ca. +1.0 and +0.35 V. Each reduction is accompanied by a simultaneous decrease in the absorbance of the film at 500 nm, indicating the reduction of the electrochromic Mn(IV) sites. At the end of the negative potential sweep, the absorbance is nearly zero, confirming the total dissolution of the original MnO_2 film. On the positive potential sweep, neither an oxidation current nor an increase in the optical absorbance is observed, indicating irreversible dissolution. Manganese oxide can be electrochemically redeposited at higher oxidation potentials as γ-MnO_2, but the original polymorph (birnessite, a layered structure) and pore architecture are not recovered.

The PPD-coated MnO_2 ambigel electrodes exhibit different electrochemical behavior with cycling in 0.1 M H_2SO_4 electrolyte (Figure 3b). The first distinction is that PPD-coated MnO_2 undergoes no electrochemical or spectroscopic changes in the potential range of +1.1 to +0.2 V over which the native MnO_2 undergoes its irreversible electrochemical dissolution process (Figure 3a). This invariance indicates that the underlying oxide in the PPD-coated MnO_2 electrode does not insert protons and electrons at the expected potentials for MnO_2 in acid electrolyte; the underlying MnO_2 is therefore effectively shielded from the acid electrolyte (specifically, H_2O and hydrated protons). A significant cathodic current begins at ca. +0.1 V (vs Ag/AgCl) and continues to the −0.4 V potential limit. This electrochemical feature is accompanied by a simultaneous decrease in the spectroscopic absorbance at 500 nm, indicating the reduction of Mn(IV) sites in the oxide. Because the reduction of the $Mn^{IV}O_2$ solid requires charge-compensating cations, we infer that protons from the acid electrolyte are transported through the PPD coating to the underlying MnO_2, at least within this limited potential range.

Minimal anodic current flows on the return sweep to positive potentials whereas the spectroscopic absorbance reaches a steady state, indicating no significant reoxidation of Mn(III) to Mn(IV) in the oxide film. However, unlike the native MnO_2, which exhibits complete dissolution and the total loss of absorbance from the initial film, the PPD-coated MnO_2 film retains most of its initial absorbance. The electrochromic response indicates that the MnO_2 solid is retained beneath the PPD coating but that the Mn(IV)/Mn(III) electrochemistry has been rectified in the hybrid configuration.

On subsequent voltammetric cycles, qualitatively similar voltammetric features for the PPD-coated MnO_2 electrode are obtained, but with diminished cathodic currents that reach steady state by the third voltammetric cycle (Figure 4a). The spectroscopic response also exhibits a loss in absorbance on the second and third cycles over the potential range of +0.2 to −0.4 V but to a much lower degree than observed on the first cycle. Although the absorbance change qualitatively tracks the loss in electrochemical current with cycling, there

Scheme 2. Proposed Electrochemical Reaction Scheme for PPD

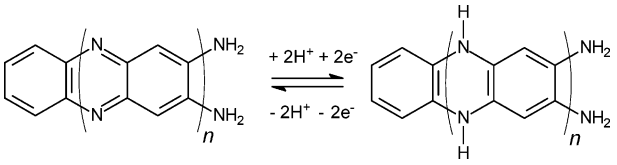

is far greater reversibility for the electrochromic processes that the optical density represents.

Under voltammetric conditions (i.e., $^{\partial E}/_{\partial t}$), the electrochemical current is proportional to the derivative of the absorbance, $i \propto {}^{\partial A}/_{\partial t}$, for electrochromic processes that adhere to the Beer−Lambert law. This method of spectroelectrochemical analysis, derivative cyclic voltabsorptometry,[39,40] may also be expressed in scan-rate-normalized terms, $^{\partial A}/_{\partial E}$ (differential absorbance). The spectroscopic response as a function of potential can thus be used to identify those features arising from electrochromic processes such as ion insertion at MnO_2. As seen in Figure 4c, the voltammetric current strongly correlates with the differential absorbance for the feature centered at −0.2 V, confirming that electrochromic processes are responsible for the observed electrochemical wave.

The potential for the redox wave at −0.2 V for the PPD-coated MnO_2 corresponds well to previous reports for the redox reactions of more conductive forms of PPD.[32,33,41−43] Although PPD has not been as thoroughly studied as other conducting polymers, there is general agreement that the redox process of PPD in aqueous acid involves a 1:1 proton/electron reaction.[32,42,44] A highly simplified mechanism for the electrochemical activity of PPD in acidic aqueous electrolytes is given in Scheme 2.[42,43] The actual reaction may involve additional protonation/deprotonation, depending on the electrolyte pH, as well as incorporation into the polymer of solvent and anions. We are currently investigating the electrochemical and electrochromic properties of PPD films prepared at planar ITO electrodes from pH 9 borate electrolyte. The PPD polymers, which deposit as self-limited insulating films from the basic monomer solution onto ITO, do exhibit voltammetric waves when cycled in acidic electrolyte (Figure 4d, dashed line).

Electrochromic Efficiencies. The spectroelectrochemical analysis of PPD-MnO_2 hybrids is also complicated by the electrochromism of the polymer film itself, which is ascribed to changes in the oxidation state of the polymer according to the reaction in Scheme 2. More highly conjugated (phenazine-like) forms of PPD exhibit anodically coloring electrochromism in the wavelength range of 350−600 nm.[33,45,46] We also observe highly reversible color changes for the self-limiting form of PPD (electrosynthesized from pH 9 monomer solution) that coincide with less-well-defined voltammetric features (Figure 4c). The similarity in the direction (anodic coloration) and wavelength range for the electrochromism of MnO_2 and PPD thus makes direct spectroelectrochemical analysis of MnO_2 difficult. The relative contributions of these two competing electrochromic responses may be qualitatively resolved by considering the electrochromic efficiency, η, which relates the change in absorbance with the amount of electrochemical charge passed. Under voltammetric conditions, the electrochromic efficiency can be determined using $\eta = ({}^{\partial A}/_{\partial t})j^{-1}$, where j is the current density.[47]

Table 1. Summary of Electrochromic Efficiency Measurements for Various MnO_2 and PPD Electrode Configurations

	electrochromic efficiency, η ($cm^2\ C^{-1}$)			
sample	$\lambda = 400$ nm	$\lambda = 450$ nm	$\lambda = 500$ nm	$\lambda = 550$ nm
PPD-ITO[a]	7 ± 1	28 ± 1	33 ± 1	17 ± 4
MnO_2[b]	16 ± 1	22 ± 1	18 ± 2	13 ± 1
PPD-MnO_2 first cycle[c]	14 ± 1	15 ± 1	12 ± 2	8 ± 2
PPD-MnO_2 second cycle[c]	6 ± 2	7 ± 2	5 ± 1	2 ± 1
PPD-MnO_2 third cycle[c]	5 ± 1	6 ± 2	5 ± 1	2 ± 1

[a] PPD film deposited potentiostatically ($E = +0.8$ V) onto a 1-cm^2 ITO electrode from a solution of 50 mM *o*-phenylenediamine in 0.1 M H_2SO_4. The electrochromic efficiency data are derived under voltammetric conditions (4 mV s^{-1}) in 0.1 M H_2SO_4. [b] Electrochromic efficiency data are derived under voltammetric conditions (4 mV s^{-1}) in 0.2 M Na_2SO_4 (pH ∼6.2). [c] Electrochromic efficiency data are derived under voltammetric conditions (4 mV s^{-1}) in 0.1 M H_2SO_4 (pH ∼6.2).

We have examined the electrochromic efficiencies of the separate components, PPD and the mesoporous MnO_2 nanoarchitecture, as well as the PPD-coated MnO_2 hybrid over the wavelength range of 400−550 nm. For the native ITO-supported MnO_2 ambigel film, the spectroelectrochemical analysis is performed in aqueous 0.2 M Na_2SO_4, in which the MnO_2 film is electrochemically stable.[12] Direct derivative cyclic voltabsorptometric analysis of the self-limiting form of PPD on ITO electrodes is problematic because the low optical density of such ultrathin films does not yield reliable measurements for η. To circumvent this problem, we used acidic conditions[48] to deposit a thicker, more conductive form of PPD on ITO electrodes, which was then examined by spectroelectrochemistry.

Electrochromic efficiencies for ITO-supported PPD and native MnO_2 ambigels are shown in Table 1 for several optical wavelengths. The MnO_2 electrodes exhibit values of η that are relatively consistent over the 400−550 nm wavelength range (varying from 13 to 22 $cm^2\ C^{-1}$). The electrochromic efficiency varies considerably over this wavelength range for ITO/PPD electrodes, from 7 $cm^2\ C^{-1}$ at 400 nm to 33 $cm^2\ C^{-1}$ at 500 nm and 17 $cm^2\ C^{-1}$ at 550 nm. When examined over a range of wavelengths, the MnO_2 and the acid-derived (more conjugated) PPD components are electrochromically distinguishable.

The same spectroelectrochemical analysis is then used to evaluate poly(*o*-phenylenediamine)-coated MnO_2 as a function of repetitive voltammetric cycles. On the first cycle for PPD-coated MnO_2, the electrochromic efficiencies range from 14 $cm^2\ C^{-1}$ at 400 nm to 8 $cm^2\ C^{-1}$ at 550 nm. Both the actual values and the distribution of η over this wavelength range are similar to those of the native MnO_2 film. For the second and third voltammetric cycles, the η values significantly decrease and are essentially invariant

with wavelength. These trends are consistent with neither the MnO_2 nor the acid-derived (more conjugated) PPD electrochromic processes. From these measurements, the electrochromic process of the first voltammetric cycle is dominated by electron−proton insertion at the underlying MnO_2 domains. We presume that both the electrochemistry and spectroscopic response of the subsequent cycles are due primarily to the overlying PPD coating but that this ultrathin, conformal version of PPD has an electrochromic efficiency that is altered relative to the isotropic morphology and more conjugated structure that arise for PPD derived from electropolymerization from acidic electrolytes.

The change in electrochromic behavior noted for the PPD-coated MnO_2 between the first and subsequent cycles is consistent with the irreversible reduction observed by cyclic voltammetry (Figure 4a). On the basis of the electrochromic measurements, we ascribe this irreversibility to proton−electron insertion at the underlying MnO_2 to form electroreduced $Mn^{III}OOH$ sites within the solid that are not reoxidized on the anodic sweep. In numerous experiments, we observe no significant electrochemical or electrochromic irreversibility for any form of the PPD polymer when electrochemically cycled in 0.1 M H_2SO_4.

On the basis of these results, we propose an electrochemical ion-gating mechanism[49,50] where proton insertion at the underlying MnO_2 electrode is metered by the redox reactions of the overlying PPD coating. The polymer coating first serves as a physical barrier to an external acidic electrolyte, specifically, H_2O and hydrated protons, and prevents the reductive dissolution observed for native MnO_2 in acidic conditions. Proton insertion at the underlying MnO_2 (with accompanying electroreduction of Mn(IV) centers) is observed only when the PPD coating itself undergoes reduction at −0.2 V (with corresponding incorporation of protons from the external electrolyte), a potential consistent with the conversion of PPD from insulating to poorly conducting. The reoxidation of Mn^{III}−OOH sites with concomitant proton expulsion occurs at potentials more positive than those where the PPD polymer is electrochemically active, presumably trapping Mn^{III}−OOH sites within the film. The actual mechanism for proton transport from external electrolyte through PPD to the encapsulated MnO_2 domains remains unknown. The mechanism may involve concerted proton−electron transfer from reduced sites in the PPD to the more highly oxidizing Mn(IV) sites within the oxide. The process may also be attributed to modulations in the protonation of the polymer coating during electrochemical cycling because each oxidation state of PPD will exhibit characteristic pK_a values. In either case, the initial and irreversible proton insertion into MnO_2 may be ascribed to the different potential ranges at which the MnO_2 (+1.0 to +0.4 V) and the PPD (0 to −0.4 V) are electrochemically active.

Conclusions. Because the ultrathin polymer allows selective transport of reactants to the high-surface-area oxide and does not occlude the porous network, these hybrids have possible use as selective sensing and catalytic nanoarchitectures. A prior report by Bartlett and co-workers used the electropolymerization of *o*-phenylenediamine at planar carbon or platinum surfaces from pH 7 lyotropic liquid crystalline electrolyte to form a thin polymer layer with an expected periodic porosity.[51] Although porosity within the polymer film could not be characterized, these authors report permselectivity for cations and also anticipate sensing possibilities with such structures. Our investigation demonstrates the feasibility of using electrochemical proton-gating polymers in a hybrid configuration with metal oxide nanoarchitectures as a new model for ultracapacitors, although a pinhole-free coating based on poly(*o*-phenylenediamine) is not an optimal choice because it cannot support reversible electrochemical cycling of the underlying MnO_2 phase. By selecting conducting polymer and metal oxide components with more favorably matched redox potentials, hybrid organic−inorganic nanoarchitectures can now be developed from low-cost metal oxides, including manganese and iron oxides, that are otherwise unstable in the high protonic conductivity media desired for ultracapacitors.

Acknowledgment. Support for this research is provided by the Office of Naval Research. We thank Paul E. Sheehan and Michael S. Doescher (NRL, code 6170) for their assistance with AFM measurements.

References

(1) Rolison, D. R. *Science* **2003**, *299*, 1698−1701.
(2) Leventis, N.; Elder, I.; Rolison, D. R.; Anderson, M. L.; Merzbacher, C. I. *Chem. Mater.* **1999**, *11*, 2837−2845.
(3) Anderson, M. L.; Stroud, R. M.; Rolison, D. R. *Nano Lett.* **2002**, *2*, 235−240.
(4) Hüsing, N.; Schubert, U. *Angew. Chem., Int. Ed.* **1998**, *37*, 22−45.
(5) Rolison, D. R.; Dunn, B. *J. Mater. Chem.* **2001**, *188*, 963−998.
(6) Leventis, N.; Elder, I. A.; Long, G. J.; Rolison, D. R. *Nano Lett.* **2002**, *2*, 63−67.
(7) Ryan, J. V.; Berry, A. D.; Anderson, M. L.; Long, J. W.; Stroud, R. M.; Cepak, V. M.; Browning, V. M.; Merzbacher, C. I.; Rolison, D. R. *Nature* **2000**, *406*, 169−172.
(8) Pietron, J. J.; Rolison, D. R. *J. Non-Cryst. Solids* **2001**, *285*, 13−21.
(9) Passerini, S.; Coustier, F.; Giorgeti, M.; Smyrl, W. H. *Electrochem. Solid State Lett.* **1999**, *2*, 483−485.
(10) Long, J. W.; Swider-Lyons, K. E.; Stroud, R. M.; Rolison, D. R. *Electrochem. Solid State Lett.* **2000**, *3*, 453−456.
(11) Long, J. W.; Stroud, R. M.; Rolison, D. R. *J. Non-Cryst. Solids* **2001**, *285*, 288−294.
(12) Long, J. W.; Young, A. L.; Rolison, D. R. *J. Electrochem. Soc.*, in press.
(13) Zheng, J. P.; Cygan, P. J.; Jow, T. R. *J. Electrochem. Soc.* **1995**, *142*, 2699−2703.
(14) Burke, L. D.; Murphy, O. J.; O'Neill, J. F.; Venkatesan, S. *J. Chem. Soc., Faraday Trans.* **1977**, *73*, 1659−1671.
(15) Tsai, E. W.; Rajeshwar, K. *Electrochim. Acta* **1991**, *36*, 27−30.
(16) Bakardjieva, S.; Bezdicka, P.; Grygar, T.; Vorm, P. *J. Solid State Electrochem.* **2000**, *4*, 306−313.
(17) Bodoardo, S.; Brenet, J.; Maja, M.; Spinelli, P. *Electrochim. Acta* **1994**, *39*, 1999−2004.
(18) Nijjer, S.; Thonstad, J.; Haarberg, G. M. *Electrochim. Acta* **2000**, *46*, 395−399.
(19) Yacynych, A. M.; Mark, H. B. *J. Electrochem. Soc.* **1976**, *123*, 1346−1351.
(20) Heineman, W. R.; Wieck, H. J.; Yacynych, A. M. *Anal. Chem.* **1980**, *52*, 345−346.
(21) White, H. S.; Abruña, H. D.; Bard, A. J. *J. Electrochem. Soc.* **1982**, *129*, 265−271.
(22) Long, J. W.; Qadir, L. R.; Stroud, R. M.; Rolison, D. R. *J. Phys. Chem. B* **2001**, *105*, 8712−8717.
(23) Conway, B. E. *J. Electrochem. Soc.* **1991**, *138*, 1539−1549.
(24) Burke, A. *J. Power Sources* **2000**, *91*, 37−50.

(25) Chabre, Y.; Pannetier, J. *Prog. Solid State Chem*. **1995**, *23*, 1−130.
(26) Thackeray, M. *Prog. Solid State Chem.* **1997**, *25*, 1−71.
(27) Pang, S.-C.; Anderson, M. A.; Chapman, T. W. *J. Electrochem. Soc*. **2000**, *147*, 444−450.
(28) Lee, H. Y.; Goodenough, J. B. *J. Solid State Chem*. **1999**, *144*, 220−223.
(29) Hu, C.-C.; Tsou, T.-W. *J. Power Sources* **2003**, *115*, 179−186.
(30) Tallman, D. E.; Spinks, G. M.; Dominis, A. J.; Wallace, G. G. *J. Solid State Electrochem.* **2002**, *6*, 73−84.
(31) Losito, I.; De Giglio; E.; Cioffi, N.; Malitesta, C. *J. Mater. Chem.* **2001**, *11*, 1812−1817 and references therein.
(32) Chiba, K.; Ohsaka, T.; Ohnuki, Y.; Oyama, N. *J. Electroanal. Chem.* **1987**, *219*, 117−124.
(33) Ogura, K.; Kokura, M.; Yano, J.; Shiigi, H. *Electrochim. Acta* **1995**, *40*, 2707−2714.
(34) Sviridov, D. V.; Kulak, A. I. *Thin Solid Films* **1991**, *198*, 191−198.
(35) Doescher, M. S.; Long, J. W.; Rolison, D. R. Unpublished results, 2003.
(36) McEvoy, T. M.; Stevenson, K. J.; Long, J. W. Unpublished results, 2002.
(37) Lee, C.-H.; Cahan, B.; Yeager, E. *J. Electrochem. Soc.* **1973**, *120*, 1689−1692.
(38) Còrdoba de Torresi, S. I.; Gorenstein, A. *Electrochim. Acta* **1992**, *37*, 2015−2019.
(39) Bancroft, E. E.; Sidwell, J. S.; Blount, H. N. *Anal. Chem.* **1981**, *53*, 1390−1394.
(40) Zamponi, S.; Czerwinski, A.; Marassi, R. *J. Electroanal. Chem.* **1989**, *266*, 37−46.
(41) Martinusz, K.; Láng, G.; Inzelt, G. *J. Electroanal. Chem.* **1997**, *433*, 1−8.
(42) Martinusz, K.; Láng, G.; Inzelt, G. *J. Electroanal. Chem.* **1994**, *379*, 437−444.
(43) Ling-Ling, W.; Luo, J.; Zhong-Hua, L. *J. Electroanal. Chem.* **1996**, *417*, 53−58.
(44) Goyette, M.-A.; Lecler, M. *J. Electroanal. Chem.* **1995**, *382*, 17−23.
(45) Wu, L.-L.; Luo, J.; Lin, Z.-H. *J. Electroanal. Chem.* **1996**, *417*, 53−58.
(46) Komura, T.; Funahasi, Y.; Yamaguti, T.; Takahasi, K. *J. Electroanal. Chem.* **1998**, *446*, 113−123.
(47) Còrodoba de Teresi, S. I. *Electrochim. Acta* **1995**, *40*, 1101−1107.
(48) In this series of experiments, PPD was electrodeposited on a bare ITO electrode (1-cm^2 geometric area) from a solution of 50 mM OPD in 0.1 M H_2SO_4.
(49) Burgmayer, P.; Murray, R. W. *J. Am. Chem. Soc*. **1982**, *104*, 6139−6140.
(50) Burgmayer, P.; Murray, R. W. *J. Phys. Chem.* **1984**, *88*, 2515−2521.
(51) Elliott, J. M.; Cabuche, L. M.; Bartlett, P. N. *Anal. Chem.* **2001**, *73*, 2855−2861.

NL0343598